Ionics (2024) 30:4091–4098
https://doi.org/10.1007/s11581-024-05553-x

RESEARCH

Nanoarchitectonics of Zn_2SnO_4/ZnO heterostructure composites for better photocatalytic performance

Wenquan Hu[1] · Wenlei Wang[1] · Zhikang Chen[1] · Qi Chen[1] · Ming Wang[1]

Received: 30 December 2023 / Revised: 27 March 2024 / Accepted: 24 April 2024 / Published online: 30 April 2024

Abstract

In this work, the Zn_2SnO_4/ZnO nanocomposites synthesized by one-step hydrothermal method had been characterized by X-ray diffraction (XRD), Fourier transform-infrared spectroscopy (FT-IR), scanning electron microscopy (SEM), high-resolution transmission electron microscopy (HR-TEM), and surface area analysis (BET) techniques, while the photocatalytic activity of the Zn_2SnO_4/ZnO had been investigated during the degradation process of organic pollutants under UV irradiation. The results indicate that the Zn_2SnO_4/ZnO displays a cube and rod-shape intertwined structure, which allows the material to maintain a large specific surface area while preserving its structural stability. The nanocomposite demonstrates a high photocatalytic activity in the degradation of methylene blue (MB), ofloxacin antibiotics (OFL), and 5% cis–trans cypermethrin emulsion (5% CTC). The heterostructure of the Zn_2SnO_4/ZnO effectively inhibited the electron–hole recombination, greatly improved the activity and stability of the catalyst, and effectively promoted the catalytic reaction.

Keywords Zn_2SnO_4/ZnO · Nanocomposites · Heterostructure · Photocatalytic activity

Introduction

Pesticide is a substance or mixture of substances used for controlling, preventing, destroying, or reducing the number of pests [1]. It can cause soil, water, and air pollution [2] and harm human [3]. Of particular concern are the widespread use of pesticides and their potential to enter water supplies and cause negative effects on public health [4]. Health care is regarded as a fundamental determining factor in development of general, physical, and mental well-being of people round the globe [5]. At the same time, a number of drugs and pharmaceuticals are emerging as serious environmental contaminants [6]. Fluro-quinolones are widely administered because of their broad-spectrum activity and exceptional tissue permeation [7]. Belonging to this class of drugs, the antibiotic ofloxacin is effective against a number of commonly occurring bacterial infections. However, its wide usage and administration are also responsible for serious contamination and health problems [8, 9]. Because of persistent and stable nature of such compounds and their metabolites, it is required to degrade such compounds by efficient degradation technologies such as heterogeneous photocatalysis [10, 11]. Most of the organic dyes and their effluents in the textile industries are toxic, carcinogenic, and have become one of the major sources of water pollution [12–14]. There are many types of wastewater treatment technologies, among which the commonly seen ones include adsorption [15], microwave catalysis, and photocatalysis. Adsorption technology is widely applicable due to its high efficiency and simplicity of operation [16]. However, after the adsorption saturation, the adsorbent needs to be regenerated or replaced [17, 18], which increases the treatment cost. Microwave catalysis technology is efficient and rapid, often more energy-efficient than traditional heating methods [19]. But the initial investment in equipment is relatively high, and not all materials are suitable for microwave catalysis, which requires specific catalysts or carriers. The semiconductor-based photocatalysis has opened up for elimination of the contaminant from the environment and has become an interesting area of research [20]. The advantage of photocatalytic technology is utilizing light energy as

✉ Wenquan Hu
huwenquan@lntu.edu.cn

✉ Ming Wang
wangming@lntu.edu.cn

[1] School of Materials Science and Engineering, Liaoning Technical University, Fuxin 123000, People's Republic of China

the driving force without generating secondary pollution, so that organic matter can be decomposed into harmless small molecules [21, 22].

Recently, tremendous efforts have been devoted to fabricate high-performance photocatalyst. A large number of inorganic semiconductors materials, especially metal oxides such as TiO_2 [23], ZnO [24], V_2O_5, BiOBr [25], CuO, Bi_2MoO_6/g-C_3N_4 [26], and metal sulfides such as Cu_2S and ZnS have been explored as photocatalyst under either UV light or visible light irradiation for this application [27]. Owing to the advantages of low cost, chemical stability, and environmental compatibility, ZnO has been widely investigated as a photo-catalyst. However, one of the main shortages for pure ZnO is that photon-generated carriers are easily recombined [28]. A large number of approaches have been reported to overcome this problem. Among them, compounded by two substances is an effective way for enhancing the photocatalytic activity [29]. Construction of semiconductor heterostructures has been as an effective strategy to enhance the photocatalytic activity [30, 31].

As important functional materials, ZnO and Zn_2SnO_4 with band gaps of 3.2 and 3.4 eV, respectively, have been intensively investigated due to their unique properties and great potential applications such as gas sensors [32], solar cells [33], and photocatalytic degradation [34]. Pure Zn_2SnO_4 typically exhibits a longer degradation time and lower efficiency when it was used for photocatalytic degradation of organic dyes such as water-soluble dyestuffs [35] and Methyl Orange (MO) [36]; the degradation rate of water-soluble dyes reached 90% in 2 h, while it took 1.5 h to degrade MO with the degradation rate of 80.3%. However, the photocatalytic performance of pure Zn_2SnO_4 can be significantly improved by coupling it with ZnO to form a Zn_2SnO_4/ZnO composite photocatalyst. It was found that the degradation rate of Zn_2SnO_4/ZnO was three times than that of pure Zn_2SnO_4 [37]. When Zn_2SnO_4 is coupled with ZnO, the heterostructure will accelerate the photogenerated electrons and holes separation and thus enhance the photocatalytic efficiency, but the photocatalytic efficiency widely depends on the surface area and the porosity of the nanostructures [38]. Although Zn_2SnO_4/ZnO composite photocatalysts have been widely studied and verified in terms of organic dye degradation, it remains relatively limited that the research on their effectiveness in degrading environmental pollutants such as pesticides and antibiotics. The widespread use of pesticides and antibiotics poses a serious threat to the environment and human health. Therefore, it is significant in exploring the potential of Zn_2SnO_4/ZnO composite photocatalysts in the degradation of these types of pollutants. In this work, the Zn_2SnO_4/ZnO heterostructured composite was prepared by a simple one-step hydrothermal method. It was studied the Zn_2SnO_4/ZnO heterostructure effect on the pollutant's degradation (methylene blue, 5% cis-cypermethrin emulsion and ofloxacin antibiotic).

Experiment sections

Materials and method

In this work, $ZnSO_4{\cdot}7H_2O$ (Aladdin, CP, grade 99.0%), $SnCl_4{\cdot}5H_2O$ (Aladdin, AR, grade 99.0%), NaOH (Aladdin, AR grade 99.0%), methylene blue (Aladdin, AR grade 99.0%), 5% cis–trans cypermethrin emulsion (Aladdin, AR grade 95.0%), ofloxacin antibiotics (Aladdin, CP, grade 99.0%), anhydrous ethanol, deionized water, and all other reagents used were analytically pure. Firstly, 1 mmol $ZnSO_4{\cdot}7H_2O$ and 0.5 mmol $SnCl_4{\cdot}5H_2O$ were added to 40 mL deionized water by stirring for 30 min. Then, 15 mmol NaOH was added to the above solution and stirred for 20 min. Finally, the above mixture was transferred to a 100-mL Teflon lined stainless steel autoclave and heated at 200 °C for 12 h. After completion, the white precipitates were collected by centrifuging at 4000 rpm and then washed for three times with deionized water and ethanol and dried at 80 °C.

Characterization

To examine the crystal quality and crystallization state of the products, the as-prepared sample was investigated by using X-ray diffraction (XRD-6100, Cukα, 40 kV). The morphologies and microstructures were characterized by scanning electron microscopy (SEM, JEOL-2100) and transmission electron microscopy (TEM, JEOL-2010). The specific surface area and pore size distribution were tested by an automatic gas adsorption analyzer (Auto Sorb-IQ). The infrared spectra were recorded at room temperature on a Fourier transform infrared spectrophotometer (IR Prestige-21) as KBr pellets in the 3500 ~ 500 cm^{-1} region.

Photocatalytic measurement

The photocatalytic activities of the products for the degradation of methylene blue (10 mg/L), 5% cis–trans cypermethrin emulsion (1 ml/L) and ofloxacin antibiotic (25 mg/L, pH=7.0) were evaluated by using photochemical reactor (QFN-GHX-I), mercury lamp light source (GY500, wavelength=315~450 nm), and UV/Vis spectrometer (Purkinje, TU-1810).

0.05 g of the as-prepared product was added in 100 mL solutions. The mixtures were continuously stirred for 1 h in the dark to ensure adsorption/desorption equilibrium. And then, the solution was exposed to UV irradiation using a 500-W mercury lamp. The solution was collected at regular

intervals to measure the dye-degradation using UV/Vis spectroscopy.

Results and discussion

Microstructure and morphology representation

The crystal structure and phase analysis of the synthesized products were investigated by XRD. As shown in Fig. 1a, all the observed diffraction peaks were consistent with the characteristic peaks of Zn_2SnO_4 and ZnO, and no other impurity peaks were detected. The diffraction peaks at 17.7°, 29.1°, 34.3°, 41.7°, 51.7°, 55.1°, and 60.4° correspond to the (111), (220), (311), (400), (422), (511) and (440) crystal planes of tetragonal Zn_2SnO_4 (PDF#74–2184). The diffraction peaks at 31.7°, 34.4°, 36.2°, 47.5°, 56.6°, 62.8°, 66.3°, 67.9°, and 69.0° corresponded to the (100), (002), (101), (102), (110), (103), (200), (112), and (201) crystal planes of the inverse spinel structure ZnO (PDF#89–0511), indicating that the product in this experiment was pure Zn_2SnO_4/ZnO. All characteristic peaks indicate that the Zn_2SnO_4/ZnO is mainly in pure spinel structure without contaminated composition.

Figure 1b is the Fourier transform infrared spectroscopy, and there are obvious absorption bands in the range of 3200 ~ 3500 cm^{-1} and 1400 ~ 1700 cm^{-1}. This corresponds to the stretching vibration absorption of the hydroxyl group (O–H) of the adsorbed water on the surface of the material. This is attributed to the large amount of hydroxyl groups and adsorbed water adsorbed on the surface of the powder. During the photocatalytic process, the photocatalyst is excited by incident photons, generating photo-generated electrons and holes. The adsorbed hydroxyl groups act as electron acceptors, effectively capturing the photo-generated electrons and suppressing their recombination with holes. This electron capture process not only prolongs the lifetime of photo-generated charge carriers but also leads to the formation of reactive species with strong oxidizing properties. These reactive species, in turn, efficiently degrade organic pollutants, thereby enhancing the overall degradation efficiency of the photocatalytic reaction. The absorption band in the range of 500 ~ 700 cm^{-1} can be attributed to the stretching vibration absorption of typical metal oxides (M–O or M–O-M, M represents Zn or Sn). In addition, the absorption band centered at 1200 cm^{-1} is attributed to the symmetric and asymmetric stretching vibrations of Zn–O-Sn. Therefore, the presence of these functional groups proves the existence of the Zn_2SnO_4/ZnO.

The results of nitrogen adsorption and desorption experiments of the Zn_2SnO_4/ZnO are shown in the Fig. 1c and d. According to the classification of the International Union of Pure and Applied Chemistry (IUPAC), the curve is a type IV isotherm, indicating that porous layer adsorption occurs. The isotherms obtained during the desorption

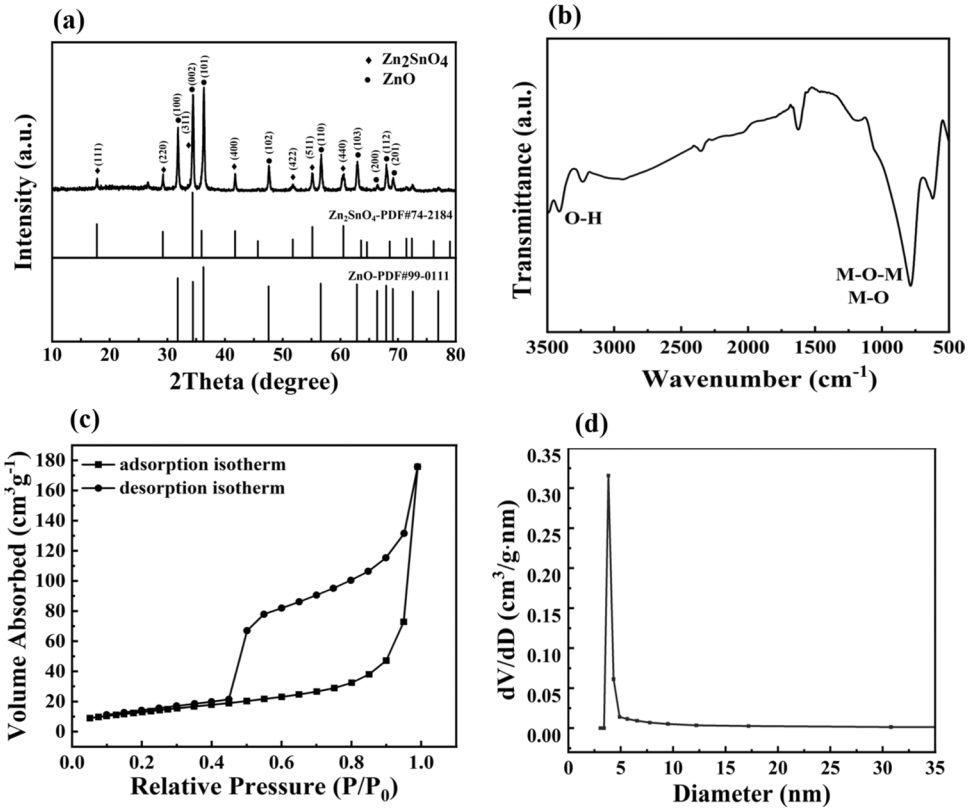

Fig. 1 **a** XRD pattern, **b** infrared spectrogram, **c** nitrogen adsorption/desorption isotherm, and **d** pore diameter distribution of the Zn_2SnO_4/ZnO

process are inconsistent with the isotherms obtained during the adsorption process. The desorption isotherm is higher than the adsorption isotherm, resulting in desorption hysteresis, showing an H3 hysteresis loop on the BJH isotherm [39]. The results show that the as-prepared Zn_2SnO_4/ZnO nanomaterials have mesopore structure. According to the BJH pore size distribution curve, there is a peak at 3.82 nm, indicating that the pore size distribution is concentrated at 3.82 nm. The specific surface areas of the Zn_2SnO_4/ZnO are obtained with 225.0 m^2/g.

The morphological information of the Zn_2SnO_4/ZnO is shown in Fig. 2a and b. It is evident that the Zn_2SnO_4/ZnO is composed of many nanocubes and nanorods. The crystal structures of Zn_2SnO_4 and ZnO are intertwined to form a unique heterojunction structure. This intertwined material exhibits excellent physical and chemical properties due to its large structural area, which facilitates the transportation and separation of charge carriers. The EDS results show that the rod-like structure predominantly features the elemental distributions of Zn and O, whereas the cubic structure demonstrates the presence of Sn, Zn, and O, which follows that Zn_2SnO_4 takes on a cubic shape, while ZnO takes on a rod shape. Elemental mapping images indicate a uniform distribution of the three elements Sn, Zn, and O that constitute Zn_2SnO_4 and ZnO, without any compositional segregation.

In order to study the detailed structure of the Zn_2SnO_4/ZnO, TEM measurement was further conducted, as shown in Fig. 2c–f. The high-resolution images shown in Fig. 2c and d allow for a clear identification of well-aligned lattice fringes. The interplanar distance of 0.317 nm corresponding to the (440) planes of Zn_2SnO_4 are indicated in Fig. 2c, while the interplanar distance of 0.24 nm corresponding to the (102) planes of ZnO is indicated in Fig. 2d. The SAED images shown in Fig. 2e and f reveal clear single-crystal electron diffraction patterns for the sample, indicating a single-crystal structure.

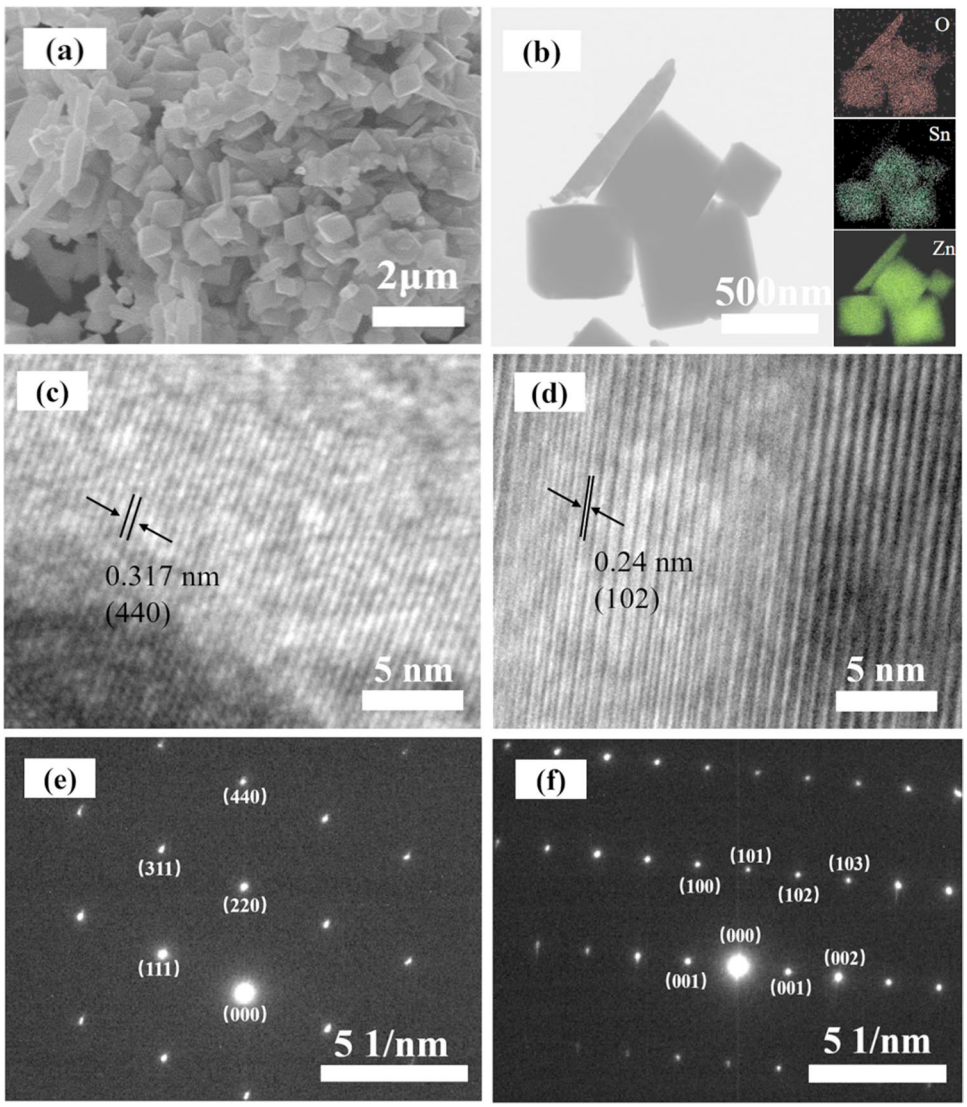

Fig. 2 **a** Scanning electron microscopy, **b** transmission electron microscopy, **c**, **d** interstitial void, and **e**, **f** selected area electron diffraction of the Zn_2SnO_4/ZnO.

Photocatalytic degradation activity

The photocatalytic activity of the as-prepared Zn_2SnO_4/ZnO was verified by photocatalytic degradation of MB, OFL, and 5% CTC, as shown in Fig. 3.

The main peak at 664 nm, 287 nm, and 194 nm are the characteristic absorption peak of MB, OFL, and 5% CTC, respectively. The peak height is proportional to the concentration of the solution. With the increase of illumination time, the color of MB solution gradually became lighter. At the same time, the unique pungent taste of 5% CTC gradually disappeared, and the OFL gradually changed from turbidity to clarification. The intensity of the characteristic absorption peak in the spectrum gradually weakened, indicating that the solution was degraded under the action of nanomaterial photocatalyst. The degradation rate can be calculated by the following formula:

$$I = \left(1 - \frac{C}{C_0}\right) \times 100\%$$

In the equation, I, C, and C_0 are the degradation rate, the real-time concentration under UV irradiation, and the initial concentration of organic dye, respectively. When calculating the final degradation rate, the C value of the solution with the longest illumination time was taken.

Figure 3a–c show the UV-absorbance spectra of Zn_2SnO_4/ZnO for degradation of MB, 5% CTC, and OFL. The

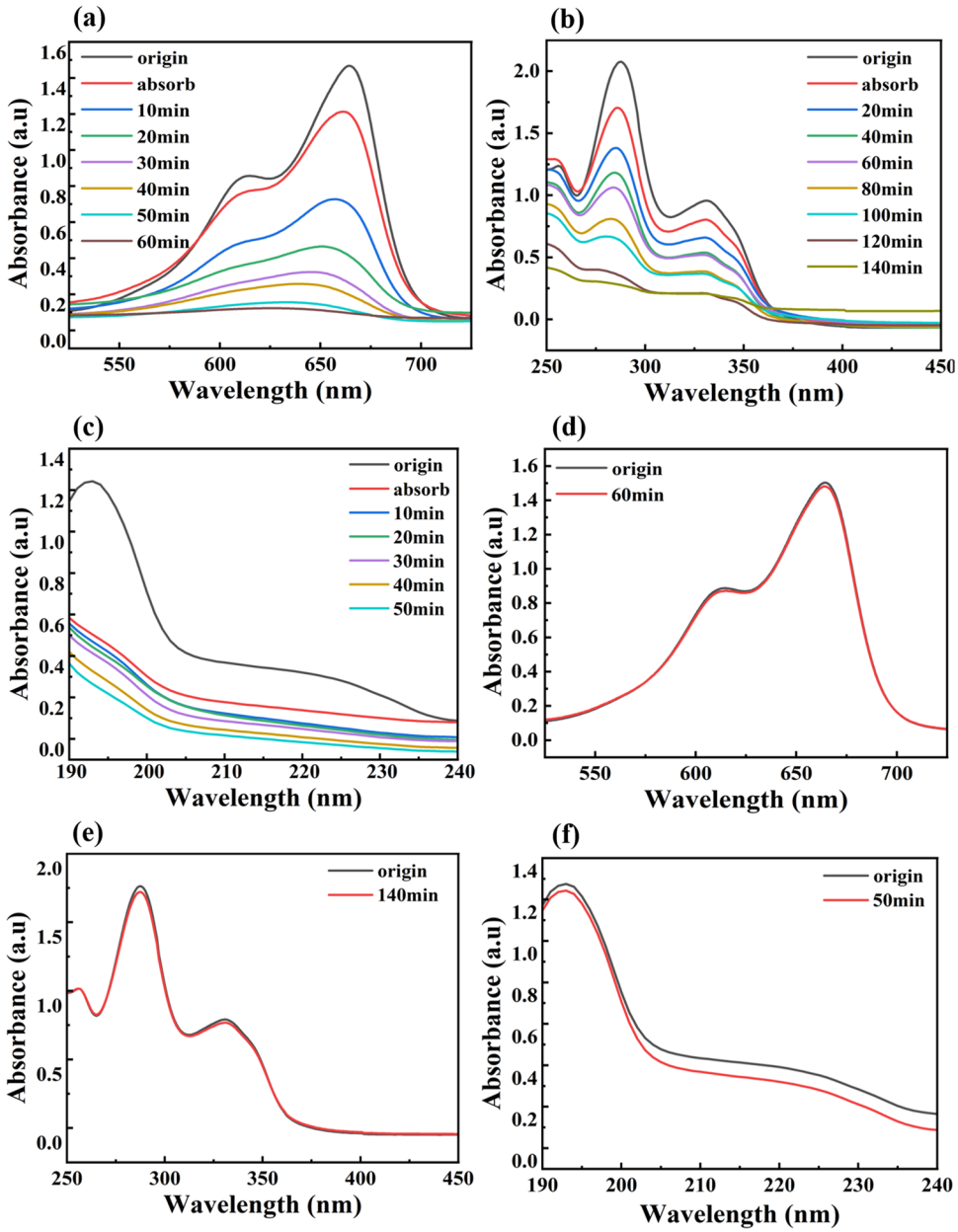

Fig. 3 Absorption spectra of several solutions in the presence of Zn_2SnO_4/ZnO photocatalyst under UV-light irradiation for different time intervals. **a** MB. **b** OFL. **c** 5% CTC. **d–f** Results of photocatalytic experiments without Zn_2SnO_4/ZnO nanomaterials

degradation rates for MB, OFL, and 5% CTC are 93.45%, 83.14%, and 86.54%, and the degradation times are 60, 140, and 50 min, respectively. The photocatalytic performance of the as-prepared Zn_2SnO_4/ZnO was better than of the reported oxide semiconductor materials [40–47]as shown in Table 1. The photocatalytic activity of the bare ZnO and bare Zn_2SnO_4 was compared with that of Zn_2SnO_4/ZnO. It can be seen that the degradation rate of MB by ZnO is only 48.3%, and the degradation rate of MB by Zn_2SnO_4 is 66.1% after 60 min as shown in Fig. 2 s, which are both lower than the 93.45% degradation rate of Zn_2SnO_4/ZnO. For the reported Zn_2SnO_4/ZnO photocatalyst [48, 49], the degradation rate for MB reached 91.5% and 60% after 120 min and 140 min, respectively. In contrast, the as-prepared Zn_2SnO_4/ZnO photocatalyst exhibits significantly superior performance in degrading MB, which the Zn_2SnO_4/ZnO achieves a higher degradation rate of 93.45% for MB after 60 min.

Generally, TiO_2 P25 is the most applied as UV light photocatalyst. In order to compare the photocatalytic performance of the as-prepared Zn_2SnO_4/ZnO with TiO_2 P25, the supplementary data on the degradation activity of MB, OFL, and 5% CTC by TiO_2 P25 as shown in Fig. 3s. The degradation rates for MB, OFL, and 5% CTC are 79.65%, 31.86%, and 55.31%, and the degradation times are 60, 140, and 50 min, respectively. It was found that the photocatalytic performance of TiO_2 P25 was lower than that of the Zn_2SnO_4/ZnO heterostructure composite.

To demonstrate that the Zn_2SnO_4/ZnO is the primary agent of degradation, this work conducted an experiment without adding the Zn_2SnO_4/ZnO as shown in Fig. 3d–f.

Table 1 Comparison of photocatalytic activities of reported oxide semiconductor materials used for photocatalytic degradation of MB, OFL, and 5% CTC

Catalyst	Source	Time/min	Degradation/%	Liquor	References
Sn_3O_4	Visible	180	33.35	MB	40
Ag-AgO/Al_2O_3	UV	90	92	MB	41
FeTi	UV	60	85	5%CTC	42
Bi/Ni-TiO_2	UV	360	70	OFL	43
Bi_2S_3/Bi_2WO_6	Visible	180	87	OFL	44
Bi_2MoO_6	Visible	90	71	OFL	45
Zn_2SnO_4	UV	60	87.3	MB	46
ZnO	UV	120	18.6	MB	47
Zn_2SnO_4/ZnO	UV	120	91.5	MB	48
Zn_2SnO_4/ZnO	UV	140	60	MB	49
Zn_2SnO_4	UV	60	66.1	MB	This work
ZnO	UV	60	48.3	MB	This work
Zn_2SnO_4/ZnO	UV	60	93.4	MB	This work
Zn_2SnO_4/ZnO	UV	140	86.5	OFL	This work
Zn_2SnO_4/ZnO	UV	50	83.1	5%CTC	This work

The characteristic absorption peak intensities of the MB, OFL, and 5% CTC were only slightly reduced. This finding indicates that UV light itself has minimal degradation properties.

Photocatalytic mechanism of the Zn_2SnO_4/ZnO is shown in Fig. 4. The conduction band (CB) and valence band (VB) potential values of ZnO and Zn_2SnO_4 are − 0.803 eV, 2.417 eV and − 0.993 eV, 2.217 eV, respectively [50]. When Zn_2SnO_4/ZnO is irradiated with UV light, Zn_2SnO_4 and ZnO can be both excited. Zn_2SnO_4/ZnO generates equal numbers of photogenerated electrons and holes. After Zn_2SnO_4 absorbs UV light, electrons transfer from valence band to conduction band, causing that photogenerated electron hole pairs are produced. Because the conduction band and valence band potential values of Zn_2SnO_4 are both lower than those of ZnO, photogenerated holes transfer from valence band of Zn_2SnO_4 to valence band of ZnO. Then, photogenerated electrons transfer from conduction band of ZnO to conduction band of Zn_2SnO_4. This greatly increases the probability of photogenerated holes and electrons migrating to the photocatalyst surface. Subsequently, the holes react with H_2O to form hydroxy radicals (·OH), while the superoxide anion radicals ($\cdot O^{2-}$) are formed by the reaction of excited electrons with absorbed oxygen. The organic dyes can be degraded by ·OH and $\cdot O^{2-}$ validly.

The Zn_2SnO_4/ZnO has good photocatalytic performance and conforms to the heterojunction transfer mode. The reasons for its good photocatalytic performance are as follows: On the one hand, the composite structure enhances the surface adsorption between the photocatalyst and the organic molecule. On the other hand, the Zn_2SnO_4/ZnO heterojunction promotes the transfer and separation of photogenerated electrons and holes, and greatly improves the photocatalytic activity.

In order to evaluate the stability and reusability of the photocatalyst, MB as a representative organic dye was chosen to degrade using recycling degradation experiment. After

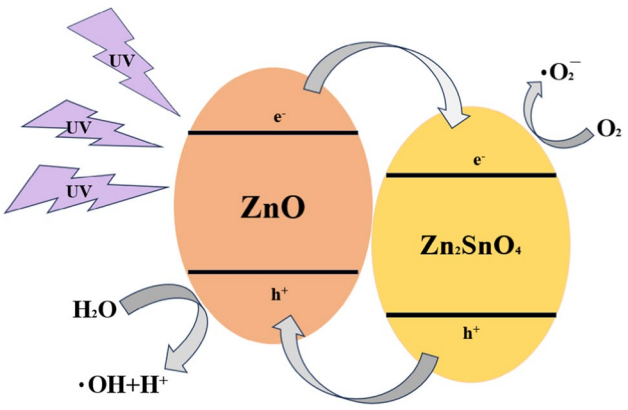

Fig. 4 Schematic diagram of charge transfer

the end of the first photocatalytic experiment, Zn_2SnO_4/ZnO was recovered by centrifugation and calcination, then carried out the photocatalytic degradation experiment again, which was repeated for 5 times. As shown in Fig. 4s, the photocatalytic degradation rates of the five experiments were 93.58%, 93.45%, 93.34%, 93.23%, and 93.16%, respectively. This reveals that there is no clear change in the degradation rate after 5 cycles, which indicates that the heterojunction system could enhance the stability of ZnO.

Conclusions

In summary, the Zn_2SnO_4/ZnO composites were successfully synthesized by a one-step hydrothermal method. The detailed characterizations reveal that the as-prepared Zn_2SnO_4/ZnO possesses pure phase, good crystallinity, and excellent photocatalytic activity for the degradation; the degradation rates for MB, OFL, and 5% CTC are 93.45%, 83.14%, and 86.54%, respectively. The as-prepared photocatalysts might have a potential application in water purification.

Supplementary Information The online version contains supplementary material available at https://doi.org/10.1007/s11581-024-05553-x.

Author contributions Wenlei Wang has done the whole work and written the entire manuscript. Wenquan Hu and Ming Wang have corrected the entire manuscript and supported the research funding. The photocatalytic experiments have been done by Zhikang Chen and Qi Chen.

Funding This work was financially supported by General Project of Science Research Foundation of Liaoning Province (LJKZ0363).

Declarations

Competing interests The authors declare no competing interests.

References

1. Tudi M, Daniel Ruan H, Wang L, Lyu J, Sadler R, Connell D, Phung DT (2021) Agriculture development, pesticide application and its impact on the environment. Int J Environ Res Public Health 18(3):1112. https://doi.org/10.3390/ijerph18031112
2. Poudel S, Poudel B, Acharya B et al (2020) Pesticide use and its impacts on human health and environment. Environ Ecosyst Sci 4(1):47–51. https://doi.org/10.26480/ees.01.2020.47.51
3. Yadav IC, Devi NL (2017) Pesticides classification and its impact on human and environment. Environ Sci Eng 6:140–158. https://doi.org/10.20546/ijcmas.2019.803.224
4. Kanan S, Moyet MA, Arthur RB, Patterson HH (2019) Recent advances on TiO_2-based photocatalysts toward the degradation of pesticides and major organic pollutants from water bodies. Catalysis Reviews. https://doi.org/10.1080/01614940.2019.1613323
5. Paul T, Dodd MC, Strathmann TJ (2010) Photolytic and photocatalytic decomposition of aqueous ciprofloxacin: transformation products and residual antibacterial activity. Water Res 44(10):3121–3132. https://doi.org/10.1016/j.watres.2010.03.002
6. Sturini M, Speltini A, Maraschi F, Profumo A, Pretali L, Irastorza EA, Albini A (2012) Photolytic and photocatalytic degradation of fluoroquinolones in untreated river water under natural sunlight. Appl Catal B 119:32–39. https://doi.org/10.1016/j.apcatb.2012.02.008
7. Kansal SK, Kundu P, Sood S, Lamba R, Umar A, Mehta SK (2014) Photocatalytic degradation of the antibiotic levofloxacin using highly crystalline TiO_2 nanoparticles. New J Chem 38(7):3220–3226. https://doi.org/10.1039/C3NJ01619F
8. Zivanovic L, Zigic G, Zecevic M (2006) Investigation of chromatographic conditions for the separation of ofloxacin and its degradation products. J Chromatogr A 1119(1–2):224–230. https://doi.org/10.1016/j.chroma.2006.02.029
9. Kundu P, Kaur A, Mehta SK, Kansal SK (2014) Removal of ofloxacin from aqueous phase using Ni-doped TiO2 nanoparticles under solar irradiation. J Nanosci Nanotechnol 14(9):6991–6995. https://doi.org/10.1166/jnn.2014.9238
10. Lode HARTMUT, Höffken G, Olschewski P, Sievers B, Kirch A, Borner K, Koeppe P (1987) Pharmacokinetics of ofloxacin after parenteral and oral administration. Antimicrob Agents Chemother 31(9):1338–1342. https://doi.org/10.1128/aac.31.9.1338
11. Wong FA, Flor SC (1990) The metabolism of ofloxacin in humans. Drug Metab Dispos 18(6):1103–1104
12. R Kant 2011 Textile dyeing industry an environmental hazard- https://doi.org/10.4236/ns.2012.41004
13. Lam SM, Sin JC, Abdullah AZ, Mohamed AR (2012) Degradation of wastewaters containing organic dyes photocatalysed by zinc oxide: a review. Desalin Water Treat 41(1–3):131–169. https://doi.org/10.1080/19443994.2012.664698
14. Wang J, Qu F, Wu X (2013) Photocatalytic degradation of organic dyes with hierarchical Ag_2O/ZnO heterostructures. Sci Adv Mater 5(10):1364–1371. https://doi.org/10.1166/sam.2013.1597
15. Gao B, Feng X, Zhang Y, Zhou Z, Wei J, Qiao R, Zhang X (2024) Graphene-based aerogels in water and air treatment: a review. Chem Eng J 149604. https://doi.org/10.1016/j.cej.2024.149604
16. Wei J, Zhang Y, Zhou Z, Bi F, Qiao R, Jiang S, Zhang X (2024) PVP-modified spindle-shaped MIL-88B (Fe) to enhance the degradation of tetracycline by activated peroxodisulfate: a comparative study and mechanistic investigation. Progress in Natural Science: Materials International 33(6):872–80. https://doi.org/10.1016/j.pnsc.2023.12.020
17. Yang Y, Jie B, Zhai Y, Zeng Y, Kang J, Cheng G, Zhang X (2024) Performance and mechanism of efficient activation of peroxymonosulfate by Co-Mn-ZIF derived layered double hydroxide for the degradation of enrofloxacin. J Mol Liq 394:123723. https://doi.org/10.1016/j.molliq.2023.123723
18. Yang Y, Jie B, Ye J, Gan F, Yu S, Lin H, Zhang X (2023) N-doped catalysts built by iron-based metal–organic framework efficiently activated peroxymonosulfate for the tetracycline degradation. J Mol Liq 392:123505. https://doi.org/10.1016/j.molliq.2023.123505
19. Wang Y, Li H, Xu J, Yu J, Wang J, Jiang H, Liu N (2024) High-performance carbon@ metal oxide nanocomposites derived metal–organic framework-perovskite hybrid boosted microwave-induced catalytic degradation of norfloxacin: performance, degradation pathway and mechanism. Sep Purif Technol 330:125399. https://doi.org/10.1016/j.seppur.2023.125399
20. Vinu R, Madras G (2010) Environmental remediation by photocatalysis. J Indian Inst Sci 90(2):189–230. https://doi.org/10.1515/ijcre-2012-0003
21. Wang Y, Li H, Xia W, Yu L, Yao Y, Zhang X, Jiang H (2023) Synthesis of carbon microsphere-supported nano-zero-valent iron sulfide for enhanced removal of Cr (VI) and p-nitrophenol complex contamination in peroxymonosulfate system. J Mol Liq 390:123089. https://doi.org/10.1016/j.molliq.2023.123089

22. Wang Y, Lin N, Xu J, Jiang H, Chen R, Zhang X, Liu N (2023) Construction of microwave/PMS combined dual responsive perovskite-MXene system for antibiotic degradation: synergistic effects of thermal and non-thermal. Appl Surf Sci 639:158263. https://doi.org/10.1016/j.apsusc.2023.158263
23. Kacem K, Casanova-Chafer J, Hamrouni A, Ameur S, Güell F, Nsib MF, Llobet E (2023) ZnO–TiO2/rGO hetero -structure for enhanced photodegradation of IC dye under natural solar light and role of rGO in surface hydroxylation. Bull Mater Sci 46(2):83. https://doi.org/10.1007/s12034-023-02913-7
24. Hamrouni A, Moussa M, Fessi N, Palmisano L, Ceccato R, Rayes A, Parrino F (2023) Solar photocatalytic activity of Ba-doped ZnO nanoparticles: the role of surface hydrophilicity. Nanomaterials 13(20):2742. https://doi.org/10.3390/nano13202742
25. Zhang J, Liu R, Kuang M, Wang J, Ji Z (2023) Effect of calcination temperature on surface acidity and photocatalytic activity of nano-TiO2/diatomite composite photocatalyst. Sci Adv Mater 15(6):781–790. https://doi.org/10.1166/sam.2023.4454
26. Su F, Huang J, Xu Y (2023) Facile fabrication of Bi_2MoO_6/g-C_3N_4 heterojunction nanosheets: facile synthesis and enhanced visible light photocatalytic property. Sci Adv Mater 15(7):905–914. https://doi.org/10.1166/sam.2023.4496
27. Barick KC, Singh S, Aslam M, Bahadur D (2010) Porosity and photocatalytic studies of transition metal doped ZnO nanoclusters. Microporous Mesoporous Mater 134(1–3):195–202. https://doi.org/10.1016/j.micromeso.2010.05.026
28. Georgekutty R, Seery MK, Pillai SC (2008) A highly efficient Ag-ZnO photocatalyst: synthesis, properties, and mechanism. J Phys Chem C 112(35):13563–13570. https://doi.org/10.1021/jp802729a
29. Li G, Gray KA (2007) The solid–solid interface: explaining the high and unique photocatalytic reactivity of TiO2-based nanocomposite materials. Chem Phys 339(1–3):173–187. https://doi.org/10.1016/j.chemphys.2007.05.023
30. Zhu YP, Li M, Liu YL, Ren TZ, Yuan ZY (2014) Carbon-doped ZnO hybridized homogeneously with graphitic carbon nitride nanocomposites for photocatalysis. J Phys Chem C 118(20):10963–10971. https://doi.org/10.1021/jp502677h
31. Sun JH, Dong SY, Feng JL, Yin XJ, Zhao XC (2011) Enhanced sunlight photocatalytic performance of Sn-doped ZnO for Methylene Blue degradation. J Mol Catal A: Chem 335(1–2):145–150. https://doi.org/10.1016/j.molcata.2010.11.026
32. Zhang Z, Xu M, Liu L, Ruan X, Yan J, Zhao W, Zhang T (2018) Novel SnO_2@ZnO hierarchical nanostructures for highly sensitive and selective NO2 gas sensing. Sens Actuators, B Chem 257:714–727. https://doi.org/10.1016/j.snb.2017.10.190
33. Song J, Zheng E, Wang XF, Tian W, Miyasaka T (2016) Low-temperature-processed ZnO–SnO_2 nanocomposite for efficient planar perovskite solar cells. Sol Energy Mater Sol Cells 144:623–630. https://doi.org/10.1016/j.solmat.2015.09.054
34. Bi F, Feng X, Zhou Z, Zhang Y, Wei J, Yuan L, Zhang X (2024) Mn-based catalysts derived from the non-thermal treatment of Mn-MIL-100 to enhance its water-resistance for toluene oxidation: mechanism study. Chem Eng J 149776. https://doi.org/10.1016/j.cej.2024.149776
35. Lou X, Jia X, Xu J, Liu S, Gao Q (2006) Hydrothermal synthesis, characterization and photocatalytic properties of Zn_2SnO_4 nanocrystal. Mater Sci Eng, A 432(1–2):221–225. https://doi.org/10.1016/j.msea.2006.06.010
36. Fu X, Wang X, Long J, Ding Z, Yan T, Zhang G, Fu X (2009) Hydrothermal synthesis, characterization, and photocatalytic properties of Zn_2SnO_4. J Solid State Chem 182(3):517–524. https://doi.org/10.1016/j.jssc.2008.11.029
37. Bai XL, Pan N, Wang XP, Wang HQ (2008) Synthesis and photocatalytic activity of one-dimensional ZnO-Zn_2SnO_4 mixed oxide nanowires. Chin J Chem Phys 21(1):81 (http://iopscience.iop.org/1674-0068/21/1/11)
38. Hamrouni A, Moussa N, Parrino F, Di Paola A, Houas A, Palmisano L (2014) Sol–gel synthesis and photocatalytic activity of ZnO–SnO_2 nanocomposites. J Mol Catal A: Chem 390:133–141. https://doi.org/10.1016/j.molcata.2014.03.018
39. Jia B, Jia W, Qu F, Wu X (2013) General strategy for self assembly of mesoporous SnO_2 nanospheres and their applications in water purification. RSC Adv 3(30):12140–12148. https://doi.org/10.1039/C3RA41638K
40. Han Y, Wei M, Qu S, Zhong M, Han L, Yang H, Lei Z (2020) Ag@AgCl quantum dots embedded on Sn3O4 nanosheets towards synergistic 3D flower-like heterostructured microspheres for efficient visible-light photocatalysis. Ceram Int 46(15):24060–24070. https://doi.org/10.1016/j.ceramint.2020.06.184
41. Motevalli K, Ebadi M, Salehi Z (2017) Synthesis of Ag–AgO/Al_2O_3 nanocomposite via a facile two-step method for photodegradation of methylene blue. J Mater Sci Mater Electron 28:13024–13031. https://doi.org/10.1007/s10854-017-7134-9
42. Solano Pizarro RA, Herrera Barros AP (2020) Cypermethrin elimination using Fe-TiO_2 nanoparticles supported on coconut palm spathe in a solar flat plate photoreactor. Adv Compos Lett 29. https://doi.org/10.1177/2633366X20906164
43. Bhatia V, Ray AK, Dhir A (2016) Enhanced photocatalytic degradation of ofloxacin by co-doped titanium dioxide under solar irradiation. Sep Purif Technol 161:1–7. https://doi.org/10.1016/j.seppur.2016.01.028
44. Adhikari S, Kim DH (2018) Synthesis of Bi_2S_3/Bi_2WO_6 hierarchical microstructures for enhanced visible light driven photocatalytic degradation and photoelectrochemical sensing of ofloxacin. Chem Eng J 354:692–705. https://doi.org/10.1016/j.cej.2018.08.087
45. Gupta G, Umar A, Kaur A, Sood S, Dhir A, Kansal SK (2018) Solar light driven photocatalytic degradation of ofloxacin based on ultra-thin bismuth molybdenum oxide nanosheets. Mater Res Bull 99:359–366. https://doi.org/10.1016/j.materresbull.2017.11.033
46. Shi L, Dai Y (2013) Synthesis and photocatalytic activity of Zn_2SnO_4 nanotube arrays. J Mater Chem A 1(41):12981–12986. https://doi.org/10.1039/C3TA12388J
47. Wang YN, Li J, Wang Q (2020) The performance of daylight photocatalytic activity towards degradation of MB by the flower-like and approximate flower-like complexes of graphene with ZnO and Cerium doped ZnO. Optik 204:164131. https://doi.org/10.1016/j.ijleo.2019.164131
48. Preethi G, Balan R, Nagaswarupa HP (2021) Hydrothermal synthesis of Zn_2SnO_4/ZnO composite for the degradation of organic pollutant Methylene Blue under UV irradiation. Mater Today Proc 47:4566–4570. https://doi.org/10.1016/j.matpr.2021.05.433
49. Lee JW, Nam SH, Yu JH, Kim DI, Jeong RH, Boo JH (2019) Morphological modulation of urchin-like Zn_2SnO_4/SnO_2 hollow spheres and their applications as photocatalysts and quartz crystal microbalance measurements. Appl Surf Sci 474:78–84. https://doi.org/10.1016/j.apsusc.2018.05.039
50. Dong S, Cui L, Tian Y, Xia L, Wu Y, Yu J, Fan M (2020) A novel and high-performance double Z-scheme photocatalyst ZnO-SnO_2-Zn_2SnO_4 for effective removal of the biological toxicity of antibiotics. J Hazard Mater 399:123017. https://doi.org/10.1016/j.jhazmat.2020.123017